Digest Journal of Nanomaterials and Biostructures Vol. 19, No. 4, October-December 2024, p. 1533-1545

Effect of substrate temperature on the physical and sensing properties of nanostructured Fe_2O_3 thin films

O. A. Chichan[a], Rusul S. Jaffer[b], S. S. Chiad[c], K. N. Hussein[d], N. F. Habubi[e], N. M. Mirza[c,*], M. Jadan[f, g], Y. H. Kadhim[h]

[a]*Department of Physics, College of Education for Pure Sciences, University of Babylon, Iraq*
[b]*Control and System Engineering Departments, University of Technology, Iraq*
[c]*Department of Physics, College of Education, Mustansiriyah University, Iraq*
[d]*Department of Radiology, Al-Manara College for Medical Science, Iraq*
[e]*Department of Radiation and Sonar Technologies, Alnukhba University College, Iraq*
[f]*Department of Physics, College of Science, Imam Abdulrahman Bin Faisal University, P.O. Box 1982, 31441 Dammam, Saudi Arabia*
[g]*Basic and Applied Scientific Research Center, Imam Abdulrahman Bin Faisal University, P.O. Box 1982, 31441 Dammam, Saudi Arabia*
[h]*Department of Optics Techniques, College of Haelth and Medical Techniques, AL-Mustaqbal University, Babylon, Hillah, 51001, Iraq*

Using Chemical Bath Deposition (CBD) Method and various substrate temperatures, Fe_2O_3 films were successfully deposited. The produced film thickness was around (320 nm). Using X-ray diffraction, researchers may examine the polycrystalline structure of Fe_2O_3 thin films. These nanofilms contain strong peaks at 2θ =32.21, suggesting a preferred orientation along the (110) plane, and the grain size increases with substrate temperature, according to XRD tests. When the base temperature was raised from 350 to 450 °C, the strain parameter decreased from 31.35 to 28.43. AFM testing of the surface morphology of the deposition of material yields excellent homogenous coatings. The findings show that the average particle size of the nanoparticles ranges from (69.8 to 32.7) nm. SEM images show Fe_2O_3 films at (350, 400, 450) °C. Increased temperature reduces grain size, influencing morphology variations. The absorbance increases with substrate temperatures and decreases rapidly at short wavelengths, which correspond to the energy gap. The transmittance increases with increasing wavelength range. It decreases with rising substrate temperatures. The band gap values vary from 2.17 eV to 2.06 eV by increasing the substrate temperatures from 350 to 450 °C. It was discovered that the band gap reduces as the temperature of the Fe_2O_3 substrate increases. In addition, the optical constants for all films, including the absorption coefficient, the refractive index, and the extinction coefficient, were computed. Fe_2O_3 film's resistance over time at 350, 400, and 450°C for 300 ppm NO_2 demonstrates oxidation effect and temperature sensitivity. Sensitivity decreases with higher base temperature due to charge carrier recombination, affecting NO_2 response.

(Received July 31, 2024; Accepted October 16, 2024)

Keywords: Fe_2O_3,thin films, XRD, AFM, Optical properties, E_g

1. Introduction

Up to 15 different iron oxide phases may be created using Fe and O [1]. These oxides, which can be produced as pure or mixed oxides, are widely distributed throughout the planet's crust. Iron oxide thin films have recently gained a lot of attention due to their intriguing magnetic properties. [2]. With a band gap of roughly (2-2.2) eV, hematite (-Fe_2O_3) is a substance that can absorb about 40% of solar energy through its visible area [3]. Iron oxide films have many different

* Corresponding author: nabeel.mirza@uomustansiriyah.edu.iq
https://doi.org/10.15251/DJNB.2024.194.1533

uses. They are suitable for gas sensors due to their high refractive index and broad bandgap [4, 5]. As a photoanode, iron oxide is recognized to exhibit intriguing characteristics [6, 7]. Moreover, thin sheets of iron oxide have been shown to have greater photo energy conversion efficiencies than commonly employed electrodes [8]. Hematite (Fe_2O_3), maghemite (Fe_2O_3), and magnetite are the most prevalent oxides (Fe_3O_4). They have various chemical, electro-optical, electrical, and magnetic characteristics. Hematite and maghemite are two of these three prevalent iron oxides used in gas sensors. For its parasitic or canted magnetic feature, hematite is widely recognized. Red pigments include it. [9, 10]; and has been tested as an electrode in photoelectrochemical (PEC) cells for energy conversion [11, 12]. High-density magnetic recording systems employ maghemite (-Fe_2O_3) [13]. Several types of magnetite (Fe_3O_4) are widely known for their giant magnetoresistance. Iron oxide nanoparticles in various phases are currently being studied. [14]. Many studies have been conducted on the shape, structure, and characteristics of -Fe_2O_3 particles [15–16]. Several fabrication methods, including sol–gel [17, 18] and PLD [19], have been employed to create iron oxide thin films. spray pyrolysis [20], RF magnetron sputtering [21], thermal evaporation technique [22], and CBD [23]. CBD makes it possible to prepare inexpensive coatings of iron oxide thin films for both small and big surfaces. This work investigates the impact of substrate temperatures on the optical characteristics of produced Fe_2O_3 films. Fe_2O_3 film's resistance over time at 350, 400, and 450°C for 300 ppm NO_2 demonstrates oxidation effect and temperature sensitivity.

2. Experimental

CBD-covered glass substrates with iron oxide thin films. Iron chloride II was the source of iron, urea served as a complexing agent, and distilled water served as the solvent. Before deposition, the glass bases were carefully cleaned with commercial detergent and washed with distilled water. The bases were cleaned and then soaked in a chromic mixture overnight before being rinsed one more with distilled water. To create a 1.0 M solution of ferrous chloride, the necessary amount of $FeCl_2.4H_2O$ was dissolved in distilled water in a 100 ml beaker. The substrates were hung vertically and submerged in the solution. After the deposition procedure, the films were annealed in an oven for four hours at 350, 450, and 500 °C. According to gravimetric measurements, the produced films had a thickness of around 320±20 nm. XRD patterns were employed to examine the structural characteristics of the films. AFM was used to investigate the films' surface morphology. SEM images were obtained using field emission scanning electron microscopy (JEOL JSM-7800F). The transmittance measurements were made using a Shimadzu spectrophotometer.
Fe_2O_3 thin films of different thicknesses (250, 300, and 350 nm) were used to construct the gas sensor with aluminum electrodes. Gas sensitivity was evaluated by measuring resistance percentage change within a cylindrical chamber (radius: 10 cm, height: 18 cm).

3. Results and discussions

Figure 1 illustrates the XRD patterns of a thin layer of Fe_2O_3 created using the Chemical Bath Deposition (CVD) technique at various substrate temperatures, with sharp peaks at 2θ equal to 33.21°, 35.73°, 49.46°, and 62.52°, respectively. These temperatures correspond to the (104), (110), (042), which is consistent with the results of the standard Fe_2O_3 X-ray diffraction data file (ICDD No. 01-089-8104). From XRD studies, it is evident that peak intensity depends on substrate temperature and suggests that the deposited Fe_2O_3 films are crystalline, consistent with what has been reported in the literature. [24,25]. More atoms can reach the substrate due to (214) planes. Additionally, this figure shows that the preferential orientation is in the direction of (110), with variations in substrate temperature resulting in thicker thin films. In a typical thin film growth process, new crystallite production and grain enlargement of previously nucleated grains co-occur under the control of deposition temperature. As seen in Fig. 1, the diffraction intensities would rise if the growth of already nucleated grains surpassed the rate at which new crystallites formed. Due

to the creation of new, smaller grains on the surface of bigger grains, the FWHM dropped as dwell duration increased. [26, 27].

The average grain size was calculated from the Scherrer formula [28]

$$D = \frac{0.9\,\lambda}{\beta cos\theta} \tag{1}$$

where λ is the wavelength of X-ray, θ is Bragg angle, and β is FWHM. As the substrate temperature increased, the full width at half maximum (FWHM) of the peaks decreased, indicating a higher degree of crystallinity. This inverse relationship between FWHM and crystallinity confirms that elevated substrate temperatures promote crystallinity. Specifically, when the base temperature was raised from 350 to 450°C, the grain size fluctuated between 11.05 and 12.19 nm [29, 30]. This suggests that higher temperatures during film deposition result in larger grain sizes, which are typically associated with improved crystallinity and structural quality [31, 32].

The formula determined the dislocation density (δ) of the Fe_2O_3 thin film as the length volume of the crystal. [33].

$$\delta = \frac{1}{D^2} \tag{2}$$

The strain (ε) was calculated by using the formula [34]:

$$\varepsilon = \frac{\beta cos\theta}{4} \tag{3}$$

As the temperature increased, the dislocation density (δ) and strain also increased, transitioning from 81.77 to 67.25 and 31.35 to 28.43, respectively. Figure 2 visually depicts these changes in dislocation density and strain. The reduction in dislocation density suggests the formation of high-quality films because both dislocation density and strain are indicators of the dislocation network within the films [35, 36]. Table 1 reveals an inverse relationship between crystalite size and other parameters. A formula utilizing the volume of the crystal was utilized to compute the δ of the Fe_2O_3 thin film.

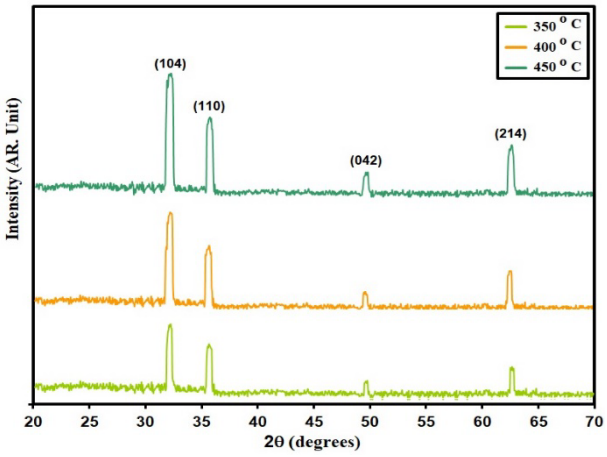

Fig. 1. XRD styles of grown films.

Table 1. D, optical bandgap and structural coefficient of grown films.

Sample (°C)	2 θ (°)	(hkl) Plane	FWHM (°)	E_g (eV)	*D* (nm)	δ (× 10^{14}) (lines/m^2)	Strain (× 10^{-4})
350	33.21	110	0.75	2.17	11.05	81.77	31.35
400	33.18	110	0.71	2.12	11.84	71.25	29.26
450	33.16	110	0.68	2.06	12.19	67.25	28.43

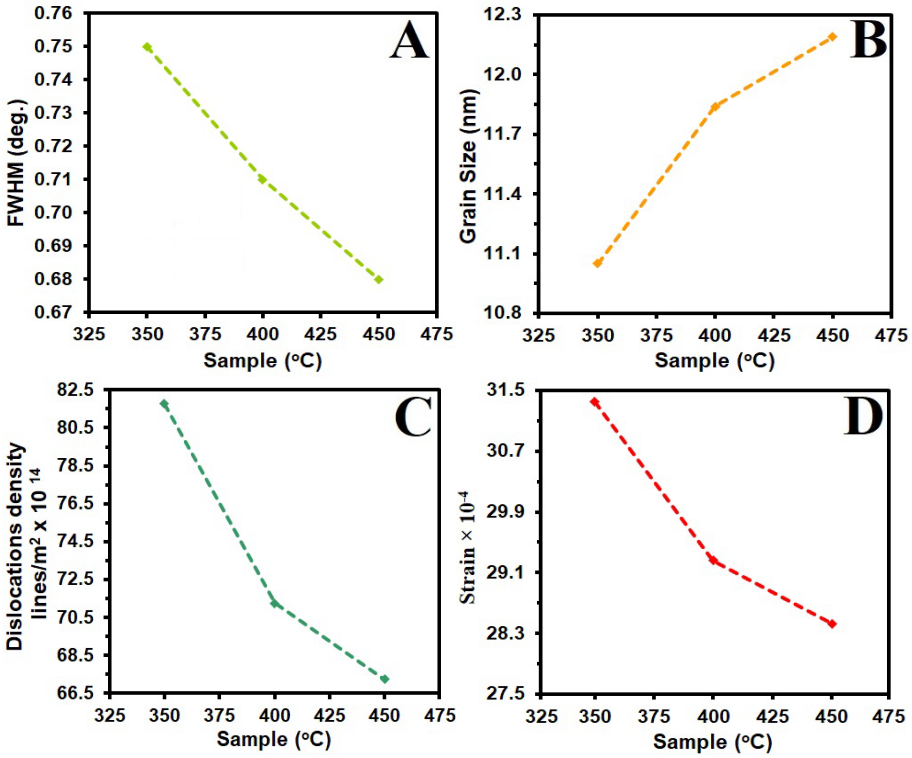

Fig. 2. FWHM (a) D (b) δ (c) ε (d) of the grown films.

XRD tests reveal that the polycrystalline film exhibits various grain sizes, as observed in the AFM (Atomic Force Microscopy) images. The AFM pictures indicate a non-compact morphology with no fractures, displaying a granular nanostructure characterized by grain sizes ranging from 69.8 to 32.7 nanometers as the base temperature increases from 350 to 450 degrees Celsius, respectively. Furthermore, it was observed that the surface roughness (Ra) decreased with the rise in substrate temperature. Table 2 provides data on the root mean square (RMS) and average roughness (Ra) of the produced films. Both RMS and Ra values show a correlation with the substrate temperature, with Ra decreasing as the temperature increases. For instance, when the substrate temperature is raised to 450 degrees Celsius, the Ra value drops from 5.6 nanometers at 350 degrees Celsius to 2.34 nanometers. This trend is consistent with the data presented in Table 2, which highlights the decrease in roughness as the substrate temperature increases. The reduction in surface roughness with increasing substrate temperature is likely attributed to the growth of crystallite size [38]. As the temperature rises, the crystallites within the film tend to grow larger, resulting in a smoother surface. This phenomenon enhances the active surface area of the samples, making them suitable materials for applications such as supercapacitors [39].

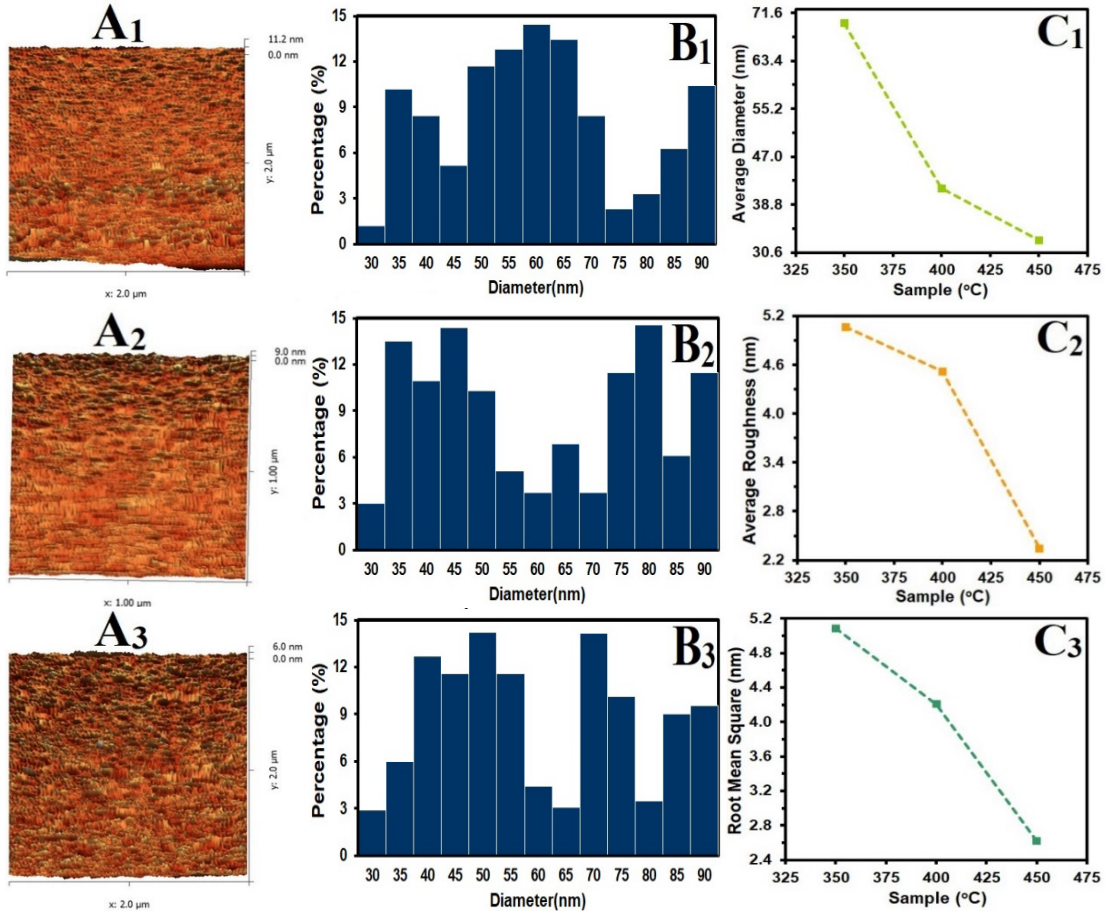

Fig. 3. AFM images (A_1, A_2 and A_3), granularly distributed (B_1, B_2 and B_3) and diversity of AFM parameters against thickness (C_1, C_2 and C_3).

Table 2. AFM parameters of the intended films.

Sample (°C)	Average Particle size nm	R_a (nm)	RMS (nm)
350	69.8	5.06	5.08
400	41.6	4.52	4.20
450	32.7	2.34	2.61

SEM images in Figure 4 (a), (b), and (c) depict the surface morphology of Fe_2O_3 thin films at substrate temperatures of (350, 400, and 450) °C. Gradual increments in substrate temperature result in reduced grain size. The surface morphology at (400 and 450) °C slightly deviates from that at 350 °C. These morphological variations may be attributed to differences in lattice structure and defects formed during deposition, influencing chemical adsorption, nucleation, and growth processes.

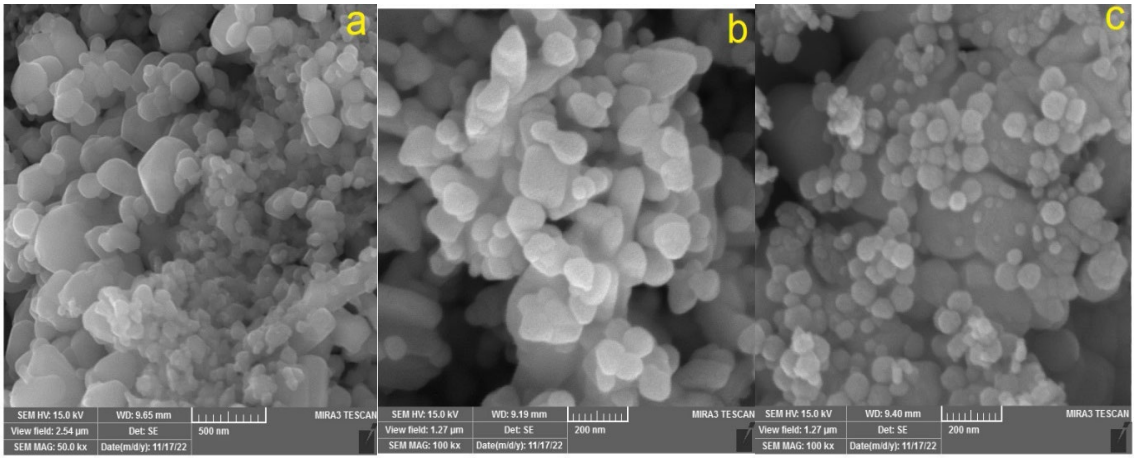

Fig. 4. SEM images of Fe_2O_3: (a) 350 °C, (b) 400 °C, (c) 450 °C.

Figure 4 displays the transmittance (T) spectra of the extended films. The graph reveals that the Fe_2O_3 thin film deposited at a substrate temperature of 450 degrees Celsius exhibits a minimum transmittance of 87% in the visible region. In contrast, the film deposited at 350 degrees Celsius shows a maximum transmittance of 93% in the near-infrared region. Reference [40] provides insight into the visible transparency quality of Fe_2O_3 thin films produced at different substrate temperatures, indicating that deposition temperatures around 350 °C are optimal for generating clear, uniform, and stoichiometric Fe_2O_3 films. Moreover, the transmission of films increases as the wavelength range expands and decreases as the temperature of the Fe_2O_3 substrate rises. As a result, the absorbance (A) is justified using the essential relationship between photon transmission and absorbance as the logarithm of the reciprocal of the transmittance. [41]:

$$A = \log 1/T \tag{4}$$

Figure 2 depicts the absorbance spectra of the Fe_2O_3 thin films (5). Due to the low energy of falling photons, the absorption spectra exhibit an exponential decrease with increasing wavelength [21]. With rising Fe_2O_3 substrate temperature, it has been shown that the highest absorption peak changes toward the longer wavelength. According to the fundamental relationship between photon transmission and absorbance, the absorbance (A) is the logarithm of the reciprocal of the transmittance in general. It increases with a rise in the temperature of the Fe_2O_3 substrate. [42, 43].

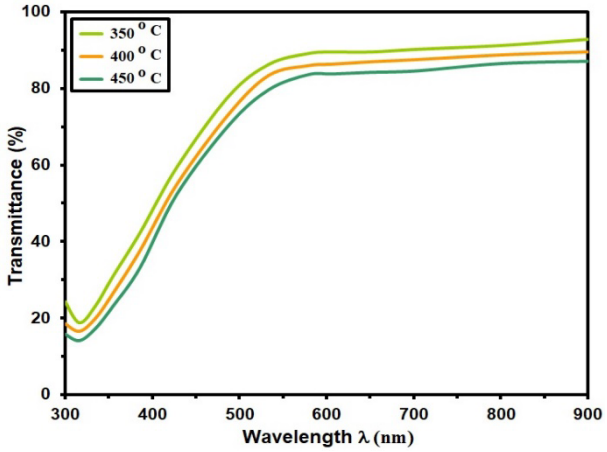

Fig. 4. T of the grown films.

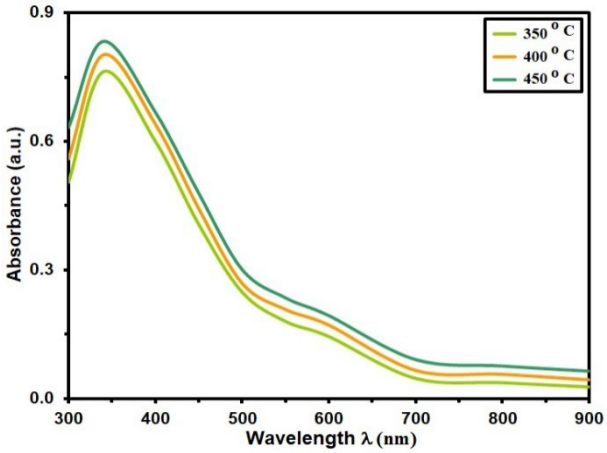

Fig. 5. Absorbance of the grown films.

Equation (5) is used to calculate the absorption coefficient (α) utilizing the analyzed date from the transmission spectrum [44]:

$$\alpha = \frac{2.303\ A}{t} \tag{5}$$

where (**t**) is the film thickness. α measured at various substrate temperatures is shown in Figure (7). It is evident that the absorption coefficient gradually increases in the high photon energy region before increasing suddenly close to the absorption edge. As a result, the value is dependent upon substrate temperature. When the substrate's temperature rises, it rises. Defective centers might cause absorption variations. The symmetry and imperfection of the lattice might alter absorption parameters [45, 46].

The energy gap (E_g) was calculated using the next equation. [47]:

$$(\alpha h\nu) = A\left(h\nu - E_g\right)^r \tag{6}$$

where hv is the photon energy (A) is constant, (r) =1/2. When substrate temperature was increased from (350, 400, and 450°C), respectively, the energy gap dropped from 3.2.17, 2.12, and 2.06 eV, as offered in Fig. 7. Due to the impact of the quantum confinement phenomena, the sample with a substrate temperature of 350 °C has a greater energy gap [48, 49]. These numbers are consistent with earlier research on Fe_3O_4 nanoparticles [50].

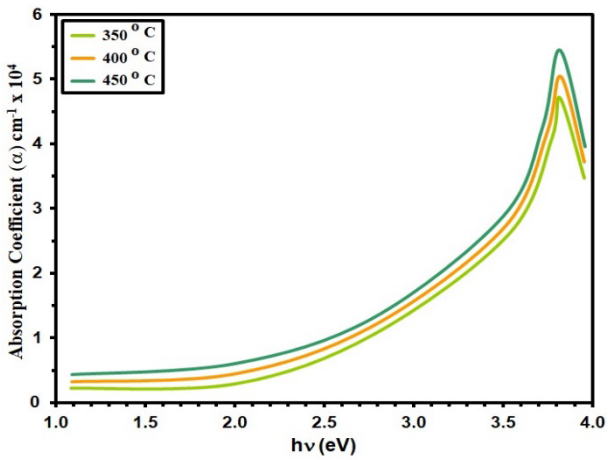

Fig. 6. α Vs hv of the prepared films.

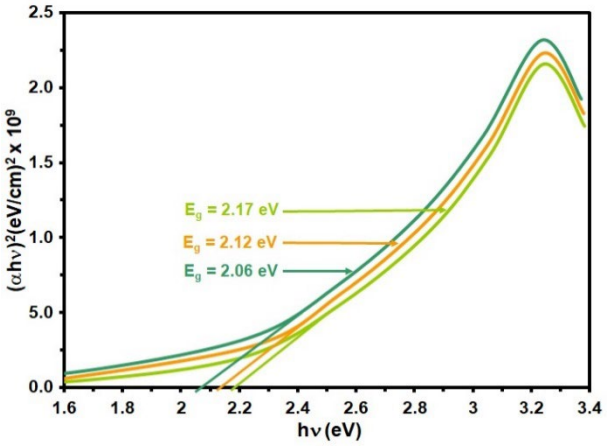

*Fig. 7. $(\alpha h\nu)^2$ versus hν of the prepared film*s.

The attenuation of an electromagnetic wave as it travels through a material is indicated by the extinction coefficient (K). The values of (K) rely on the material's free electron density and any structural flaws. Using the connection, the extinction coefficient was assessed. [51]:

$$k = \frac{\alpha\lambda}{4\pi} \tag{8}$$

and by the relationship, k and α are directly connected. For all thin films made of (Fe_2O_3), the change in extinction coefficient is offered in Figure 8. Given that the previous connection connects k and α, it is evident that k acts similarly to the latter. Due to the acceleration of crystallite development, the extinction coefficient drops as the substrate temperature rises. [52, 53].

The index of refractive (n) could be derived from Eq. (9) [46]:

$$n = \left(\frac{1+R}{1-R}\right) + \sqrt{\frac{4R}{(1-R)^2} - k^2} \tag{9}$$

The link between refractive index and wavelength, calculated using relation, is shown in Fig (9). The wavelengths have an impact on the refractive indices. Between 3.28 and 3.12 is the refractive index range, and it falls when the Fe_2O_3 substrate temperature rises from 350 to 450 oC. These declines are brought on by an overall rise in reflectance as the temperature of the Fe_2O_3 substrate rises. [55].

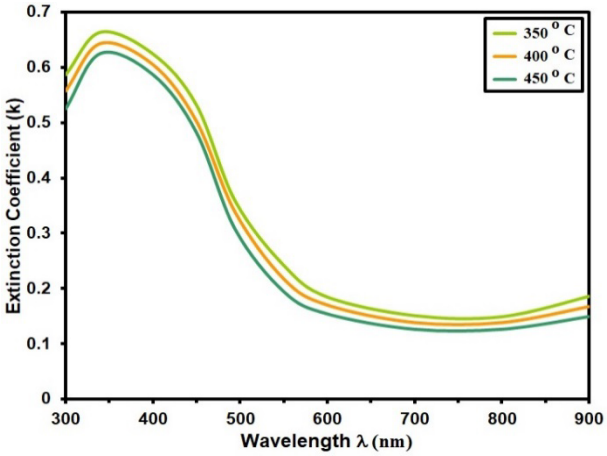

Fig. 8. k of the grown films.

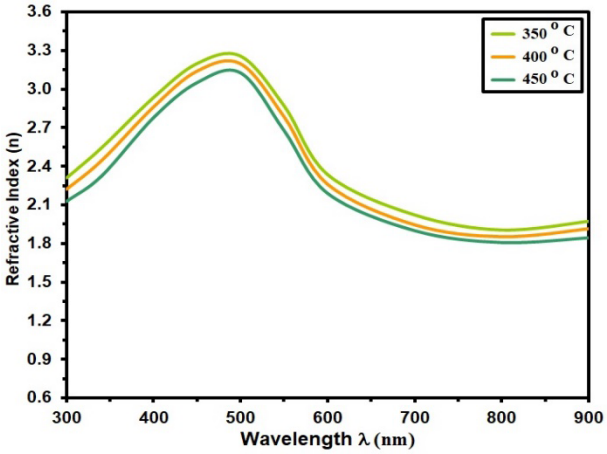

Fig. 9. n for grown films.

In Figure (11), the depicted trend shows the resistance over time of Fe_2O_3 film at base temperatures of 350, 400, and 450°C for 300 ppm of NO_2 at an operating temperature of 90°C. This demonstrates the effect of NO_2 molecules, initiating surface oxidation. This process involves the release of bonded electrons by specific O^{2+} ions, leading to electron drift back to the conduction band [56, 57]. Consequently, this electron drift increases resistance and strengthens the potential barrier under these conditions [49, 50]. Notably, at a base temperature of 450°C, the Fe_2O_3 film displays the highest resistance (R), indicating a direct association with film sensitivity and robust resistance to gas flow [58].

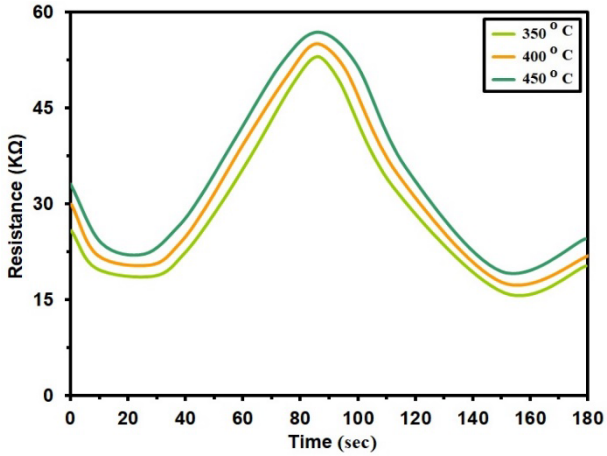

Fig. 11. Dynamic resistance change of Fe_2O_3 film at 350, 400 and 450 °C base temperatures.

The detection sensitivity, or sensor response, can be determined utilizing the equation [59]:

$$Sensitivity = \frac{\Delta R}{R_g} = \left|\frac{R_g - R_a}{R_g}\right| \times 100\ \% \tag{10}$$

Figure (13) depicts changes in sensor sensitivity with different base temperatures (350, 400, and 450) °C post-exposure to NO_2 gas. The decrease in sensitivity with increasing base temperature is attributed to charge carrier recombination between holes and electrons released from oxygen, leading to increased film electrical resistance [60, 61]. At base temperatures (350, 400, and 450) °C, sensitivity declined from 58.2% to 34.3% for 300 ppm, from 56.4% to 32.2%

for 200 ppm, and from 54.3% to 29.9% for 100 ppm [62]. These trends indicate a complex relationship between base temperatures, film sensitivity, and response to various NO_2 gas concentrations.

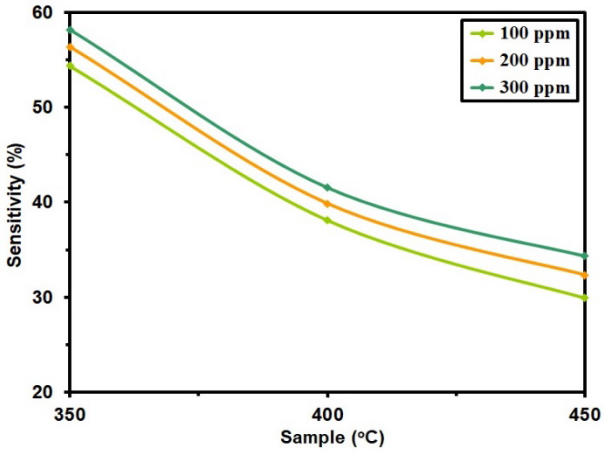

Fig. 12. Sensitivity of Fe_2O_3 film at 350, 400 and 450 °C base temperatures.

4. Conclusion

The thickness of the obtained films was around for the Fe_2O_3 thin films made by Chemical Bath Deposition (CVD) technique at various substrate temperatures (320 nm). The films that were deposited had a crystalline phase, according to XRD data. The (110) preferred orientation is improved by increasing the substrate temperature ratio, and XRD examination has validated the Fe_2O_3 nanostructure in all samples. When the base temperature was raised from 350 to 450 °C, the grain size of Fe_2O_3 grew from 11.05 nm to 12.19 nm, while the strain increased from 31.35 to 28.43.AFM pictures as substrate temperatures rise from 350 to 450 °C and surface roughness decreases from 5.06 nm to 2.34 nm. SEM images show Fe_2O_3 films at substrate temperatures (350, 400, 450) °C. Increased temperature reduces grain size, influencing morphology. The optical properties revealed that all films' transmittance increased as the wavelength range expanded and decreased as the Fe_2O_3 substrate temperature increased. A Fe_2O_3 thin film with a substrate temperature of 350 °C has a maximum transmittance of 93% in the near-infrared region and a minimum transmittance of 87% in the visible region. Band gap values vary between 2.17 eV and 2.06 eV for Fe_2O_3 substrate temperatures between 350 and 450 °C. Fe_2O_3 film resists NO_2 oxidation, showing highest resistance at 450°C—decreased sensitivity at higher base temperatures due to charge carrier recombination, affecting NO_2 response.

Acknowledgements

The authors thank Mustansiriyah University and Alnukhba University College for the financial support of this research.

References

[1] M. Abaker, U. Ahmad, S. Baskoutas, G.N. Dar, S.A. Zaidi, S.A. Al-Sayari, A. Al-Hajry, S.H.Kim, S.W. Hwang, Journal of Physics D: Applied Physics, 44, 425401(2011); https://doi.org/10.1088/0022-3727/44/42/425401/meta

[2] V. M. Aroutiounian, V.M. Arakelyan, G.E. Shahnazaryan, Solar Energy, 78 (2005) 581-592,

https://doi.org/10.1016/j.solener.2004.02.002
[3] X. Lai, G. Shen, P. Xue, B. Yan, H. Wang, P. Li, W. Xia, J. Fang, Nanoscale, 7, 4005-4012 (2015); https://doi.org/10.1039/C4NR05772D
[4] C. Xia, C. Hu, Y. Xiong, N. Wang, Journal of Alloys and Compounds, 480, 970-973 (2009); https://doi.org/10. 1016/j.jallcom.2009.02.106
[5] Bandgar, D., Navale, S., Khuspe, G., Pawar, S., Mulik, R., Patil, V., Materials Science in Semiconductor Processing 17, 67-73 (2014); https://doi.org/10.1016/j.mssp.2013.08.016
[6] Bandgar, D., Navale, S., Mane, A., Gupta, S., Aswal, D., Patil, V., 2015 Synthetic Metals 204, 1-9 (2015); https://doi.org/10.1016/j.synthmet.2015.02.032
[7] Hao, Q., Li, L., Yin, X., Liu, S., Li, Q., Wang, T., Materials Science and Engineering: B 176, 600-605 (2011); https://doi.org/10.1016/j.mseb.2011.02.002
[8] Huo, L., Li, Q., Zhao, H., Yu, L., Gao, S., Zhao, J., Sensors and Actuators B: Chemical 107, 915-920 (2005); https://doi.org/10.1016/j.snb.2004.12.046
[9] Rasheed, H. S., K. M. Qader, K. N. Hussein, N. F. Habubi, S. S. Chiad, N. M. Mirza, M. Jadan, Y. H. Kadhim, Digest Journal of Nanomaterials & Biostructures (DJNB) 19 (2), 805-818 (2024); https://doi.org/10.15251/DJNB.2024.192.805
[10] N. Song, H. Jiang, T. Cui, L. Chang, X. Wang, Nano Letters, Institution of Engineering and Technology, 943-946 (2012); https://doi.org/10.1049/mnl.2012.0631
[11] J. Chen, L. Xu, W. Li, X. Gou, Advanced Materials, 17. 582-586 (2005).
[12] C. Wang, L. Yin, L. Zhang, D. Xiang, R. Gao, Sensors, 10 (2010); https://doi.org/10. 10.3390/s100302088
[13] S. K. Muhammad, M. O. Dawood, N. Y. Ahmed, E. S. Hassan, N. F. Habubi, S. S. Chiad, Journal of Physics: Conference Series, 1660 (1), 012057 (2020); https://doi.org/10.1088/1742-6596/1660/1/012057
[14] M. R. Belkhedkar, A.U. Ubale, Y.S. Sakhare, N. Zubair, M. Musaddique, Journal of the Association of Arab Universities for Basic and Applied Sciences, 21, 38-44 (2016); https://doi.org/10.1016/j.jaubas.2015.03.001
[15] S. S. Chiad, K. H. Abass, T. H. Mubarak, N. F. Habubi, M. K. Mohammed, A. A. , Khadayeir, Journal of Global Pharma Technolog, 11(4), 369-375 (2019).
[16] M. Tadić, D. Marković, V. Spasojević, V. Kusigerski, M. Remškar, J. Pirnat, Z. Jagličić, Journal of Alloys and Compounds, 441, 291-296 (2007); https://doi.org/10.1016/j.jallcom.2006.09.099
[17] Kan-Rong Lee et al, Int. J. Electrochem. Sci. 9, 7680-7692 (2014); https://doi.org/10.1016/S1452-3981(23)10997-7
[18] C.D. Park, D. Magana, A. E. Chem. Mater. 19, 677-683 (2007); https://doi.org/10.1021/cm0617079
[19] A. K. Elttayef, M. H. Jaduaa , M. A. Muhammed, International Journal of Application or Innovation in Engineering & Management (IJAIEM), 4 (4) 99-105, (2015).
[20] Negar Khademi, M. M. Bagheri-Mohagheghi, Thermal Energy and Power Engineering. 2, 89-93(2013); https://doi.org/10.1016/j.jallcom.2013.05.057
[21] X.W. Li, A. Gupta, G. Xiao, G.Q. Gong, J. Appl. Phys. 83, 7049-7051(1998); https://doi.org/10.1063/1.367547
[22] A.Z. Moshfegh, R. Azimirad, O. Akhavan, Thin Solid Films. 484, 124-131 (2005); https://doi.org/10.1016/j.tsf.2005.02.019
[23] E.L. Miller, D. Paluselli, B. Marsen, R.E. Rocheleau, Solar Energy Mater. And Solar Cells. 88, 131-144 (2005); https://doi.org/10.1016/j.solmat.2004.07.058
[24] E. H. Hadi, D. A. Sabur, S. S. Chiad, N. F. Habubi, K., Abass, Journal of Green Engineering, 10 (10), 8390-8400 (2020); https://doi.org/10.1063/5.0095169

[25] K. Y. Qader, R. A. Ghazi, A. M. Jabbar, K. H. Abass, S. S. Chiad, Journal of Green Engineering, 10 (10), 7387-7398 (2020); https://doi.org/10.1016/j.jece.2020.104011
[26] R. I. Jasim, E. H. Hadi, S. S. Chiad, N. F. Habubi, M. Jadan, J. S. Addasi, Journal of Ovonic Research, 19 (2), 187 – 196 (2023); https://doi.org/10.15251/JOR.2023.192.187
[27] K. S. Sharba, A. S. Alkelaby, M. D. Sakhil, K. H. Abass, N. F. Habubi, S. S. Chiad, NeuroQuantology, 18 (3), 66-73 (2020); https://doi.org/10.14704/NQ.2020.18.3.NQ20152
[28] A. A. Khadayeir, E. S. Hassan, S. S. Chiad, N. F. Habubi, K. H. Abass, M. H. Rahid, T. H. Mubarak, M. O. Dawod, I. A. Al-Baidhany, Journal of Physics: Conference Series 1234 (1), 012014, (2019); https://doi.10.88/1742-6596/1234/1/012014
[29] Hassan, E.S., Mubarak, T.H., Chiad, S.S., Habubi, N.F., Khadayeir, A.A., Dawood, M.O., Al-Baidhany, I. A. , Journal of Physics: Conference Series, 1294(2), 022008 (2019); https://doi.10.88/1742-6596/1294/2/022008
[30] M.O. Dawood, S.S. Chiad, A.J. Ghazai, N.F. Habubi, O.M. Abdulmunem, AIP Conference Proceedings 2213, 020102,(2020); https://doi.org/10.1063/5.0000136
[31] H. T. Salloom, R. I. Jasim, N. F. Habubi, S. S. Chiad, M. Jadan, J. S. Addasi, Chinese Physics B, 30 (6), 068505 (2021); https://doi.org/10.1088/1674-1056/abd2a7
[32] S. S Chiad,, A. S. Alkelaby, K. S. Sharba,, Journal of Global Pharma Technology, 11 (7), 662-665, (2020); https://doi.org/10.1021/acscatal.1c01666
[33] Chiad, S.S., Noor, H.A., Abdulmunem, O.M., Habubi, N.F., Journal of Physics: Conference Series 1362(1), 012115 (2019); https://doi.org/10.1088/1742-6596/1362/1/012115
[34] K. Y. Qader, E. H. Hadi, N. F. Habubi, S. S. Chiad, M. Jadan, J. S. Addasi, International Journal of Thin Films Science and Technology, 10 (1), 41-44 (2021); https://doi.org/ 10.18576/ijtfst/100107
[35] N. N. Jandow, M. S. Othman, N. F.Habubi, S. S. Chiad, K. A. Mishjil, I. A. Al-Baidhany, Materials Research Express, 6 (11), (2020); https://doi.org/10.1088/2053-1591/ab4af8
[36] M. D. Sakhil, Z. M. Shaban, K. S. Sharba, N. F. Habub, K. H. Abass, S. S. Chiad, A. S. Alkelaby, NeuroQuantology, 18 (5), 56-61 (2020); https://doi.org/10.14704/nq.2020.18.5.NQ20168
[37] E. S. Hassan, K. Y. Qader, E. H. Hadi, S. S. Chiad, N. F. Habubi, K. H. Abass, Nano Biomedicine and Engineering, 12(3), pp. 205-213 (2020); https://doi.org/10.5101/nbe.v12i3.p205-213
[38] M. S. Othman, K. A. Mishjil, H. G. Rashid, S. S. Chiad, N. F. Habubi, I. A. Al-Baidhany, Journal of Materials Science: Materials in Electronics, 31(11), 9037-9043 (2020); https://doi.org/10.1007/s10854-020-03437-0
[39] B. A. Bader, S. K. Muhammad, A. M. Jabbar, K. H. Abass, S. S. Chiad, N. F. Habubi, J. Nanostruct, 10(4): 744-750, (2020); https://doi.org/ 10.22052/JNS.2020.04.007
[40] F. H. Jasim, H. R. Shakir, S. S. Chiad,N. F. Habubi, Y. H. Kadhi, Jadan, M., Digest Journal of Nanomaterials and Biostructures, 18(4), 1385–1393 (2023); https://doi.org/10.15251/DJNB.2023.184.1385
[41] E. S. Hassan, D. M. Khudhair, S. K. Muhammad, A. M. Jabbar, M.O. Dawood, N. F. Habubi, S. S. Chiad, Journal of Physics: Conference Series ,1660 (1) 1660 012066 (2020); https://doi.org/10.1088/1742-6596/1660/1/012066
[42] A. S. Al Rawas, M. Y. Slewa, B. A. Bader, N. F. Habubi, S. S. Chiad, Journal of Green Engineering,10 (9), 7141-7153 (2020); https://doi.org/10.1021/acsami.1c00304
[43] R. S. Ali, H. S. Rasheed, N. F. Habubi, S.S. Chiad, Chalcogenide Letters,, 20 (1), 63–72 (2023; https://doi.org/10.15251/CL.2023.201.63
[44] A. S. Alkelaby, K. H. Abass, T. H. Mubarak, N. F. , Habubi, S. S. Chiad, I. Al-Baidhany, Journal of Global Pharma Technology 11(4), 347-352 (2019).
[45] N. Y. Ahmed, B. A. Bader, M. Y. Slewa, N. F. Habubi, S. S. Chiad, NeuroQuantology, 18(6), 55-60 (2020); https://doi.org/10.1016/j.jlumin.2021.118221
[46] A. A. Khadayeir, K. H. Abass, S. S. Chiad, M. K. Mohammed, N. F. Habubi, T. K. Hameed, I. A. Al-Baidhany, Journal of Engineering and Applied Sciences, 13 (22), 9689-9692 (2018).
[47] A. Ghazai, K. Qader, N. F. Hbubi, S. S. Chiad, O. Abdulmunem, IOP Conference Series: Materials Science and Engineering, 870 (1), 012027 (2020); https://doi.org/10.1088/1757-899X/870/1/012027

[48] R. S. Ali, M. K. Mohammed, A. A. Khadayeir, Z. M. Abood, N. F. Habubi and S. S. Chiad, Journal of Physics: Conference Series, 1664 (1), 012016 (2020); https://doi:10.1088/1742-6596/1664/1/012016
[49] A. A. Khadayeir, R. I. Jasim, S. H. Jumaah, N. F, Habubi, S. S. Chiad, Journal of Physics: Conference Series,1664 (1) (2020); https://doi.org/10.1088/1742-6596/1664/1/012009
[50] O. M. Abdulmunem, A. M. Jabbar, S. K. Muhammad, M. O. Dawood, S. S. Chiad, N. F. Habubi, Journal of Physics: Conference Series,1660 (1), 012055 (2020); https://doi.org/10.1088/1742-6596/1660/1/012055
[51] E. H. Hadi, M. A. Abbsa, A. A. Khadayeir, Z. M. Abood, N. F. Habubi, and S.S. Chiad, Journal of Physics: Conference Series, 1664 (1), 012069 (2020); https://doi.org/10.1088/1742-6596/1664/1/012069
[52] Khadayeir, A. A., Hassan, E. S., Mubarak, T. H., Chiad, S.S., Habubi, N. F., Dawood, M.O., Al-Baidhany, I. A., Journal of Physics: Conference Series, 1294 (2) 022009(2019); https://doi.1088/1742-6596/1294/2/022009
[53] A. J. Ghazai, O. M. Abdulmunem, K. Y. Qader, S. S. Chiad, N. F. Habubi, AIP Conference Proceedings 2213 (1), 020101 (2020); https://doi.org/10.1063/5.0000158
[54] H. A. Hussin, R. S. Al-Hasnawy, R. I. Jasim, N. F. Habubi, S. S. Chiad, Journal of Green Engineering, 10(9), 7018-7028 (2020); https://doi.org/10.1088/1742-6596/1999/1/012063
[55] S. S. Chiad, H. A. Noor, O. M. Abdulmunem, N. F. Habubi, M. Jadan, J. S. Addasi, Journal of Ovonic Research, 16 (1), 35-40 (2020). https://doi.org/10.15251/JOR.2020.161.35
[56] H. T. Salloom, E. H. Hadi, N. F. Habubi, S. S. Chiad, M. Jadan, J. S. Addasi, Digest Journal of Nanomaterials and Biostructures, 15 (4), 189-1195 (2020); https://doi.org/10.15251/DJNB.2020.154.1189
[57] R. S Ali, N. A. H. Al Aaraji, E. H. Hadi, N. F. Habubi, S. S. Chiad, Journal of Nanostructuresthis link is disabled, 10(4), 810–816 (2020); https://doi.org/10.22052/jns.2020.04.014
[58] F. A. Jasima , Z. S. A. Mosa, N. F. Habubi, Y. H. Kadhim, S. S. Chiad, Digest Journal of Nanomaterials and Biostructures, 18 (3), 1039–1049 (2023); https://doi.org/10.15251/DJNB.2023.183.1039
[59] S. K. Muhammad, N. D. M. Taqi, S. S. Chiad, K. H. Abass, N. F. Habubi, Journal of Green Engineering, 11(2), 1287-1299 (2021).
[60] A. A. Abdul Razaq, F. H. Jasim, S. S. Chiad F. A. Jasim, Z. S. A. Mosa , Y. H. Kadhimd, Journal of Ovonic Research, 20 (2), 131 – 141 (2024); https://doi.org/10.15251/JOR.2024.202.131
[61] M. G. Brik, C. G. Ma, Comput. Mater. Sci., 51, 380-388 ((2012); https://doi.org/10.1016/j.commatsci.2011.08.008
[62] T. Sugimoto, A. Muramatsu, K. Sakata, D. Shindo, Journal of Colloid and Interface Science, 158, 420-428(1993); https://doi.org/10.1006/jcis.1993.1274